The Journal of Immunology

Identification of a Potent Microbial Lipid Antigen for Diverse NKT Cells

Benjamin J. Wolf, Raju V. V. Tatituri, Catarina F. Almeida, Jérôme Le Nours, Veemal Bhowruth, Darryl Johnson, Adam P. Uldrich, Fong-Fu Hsu, Manfred Brigl, Gurdyal S. Besra, Jamie Rossjohn, Dale I. Godfrey and Michael B. Brenner

J Immunol published online 7 August 2015
http://www.jimmunol.org/content/early/2015/08/06/jimmunol.1501019

The Journal of Immunology is published twice each month by The American Association of Immunologists, Inc., 9650 Rockville Pike, Bethesda, MD 20814-3994.

Print ISSN: 0022-1767 Online ISSN: 1550-6606.

Published August 7, 2015, doi:10.4049/jimmunol.1501019

Identification of a Potent Microbial Lipid Antigen for Diverse NKT Cells

Benjamin J. Wolf,* Raju V. V. Tatituri,* Catarina F. Almeida,[†,‡] Jérôme Le Nours,[§,¶] Veemal Bhowruth,[‖] Darryl Johnson,[†,‡] Adam P. Uldrich,[†,‡] Fong-Fu Hsu,[#] Manfred Brigl,[**] Gurdyal S. Besra,[‖] Jamie Rossjohn,[§,¶,††] Dale I. Godfrey,[†,‡] and Michael B. Brenner*

Semi-invariant/type I NKT cells are a well-characterized CD1d-restricted T cell subset. The availability of potent Ags and tetramers for semi-invariant/type I NKT cells allowed this population to be extensively studied and revealed their central roles in infection, autoimmunity, and tumor immunity. In contrast, diverse/type II NKT (dNKT) cells are poorly understood because the lipid Ags that they recognize are largely unknown. We sought to identify dNKT cell lipid Ag(s) by interrogating a panel of dNKT mouse cell hybridomas with lipid extracts from the pathogen *Listeria monocytogenes*. We identified *Listeria* phosphatidylglycerol as a microbial Ag that was significantly more potent than a previously characterized dNKT cell Ag, mammalian phosphatidylglycerol. Further, although mammalian phosphatidylglycerol-loaded CD1d tetramers did not stain dNKT cells, the *Listeria*-derived phosphatidylglycerol-loaded tetramers did. The structure of *Listeria* phosphatidylglycerol was distinct from mammalian phosphatidylglycerol because it contained shorter, fully-saturated anteiso fatty acid lipid tails. CD1d-binding lipid-displacement studies revealed that the microbial phosphatidylglycerol Ag binds significantly better to CD1d than do counterparts with the same headgroup. These data reveal a highly potent microbial lipid Ag for a subset of dNKT cells and provide an explanation for its increased Ag potency compared with the mammalian counterpart. *The Journal of Immunology*, 2015, 195: 000–000.

Natural killer T cells are a subset of αβ TCR^+ T cells that recognize lipids presented by the MHC class I–like molecule CD1d (1). These cells are divided into two categories based upon TCR usage: semi-invariant/type I NKT (iNKT) cells and diverse/type II NKT (dNKT) cells. iNKT cells primarily express an invariant TCRα-chain (Vα24-Jα18 in human, Vα14-Jα18 in mice) complexed with a limited repertoire of TCRβ-chains, whereas dNKT cells typically express diverse TCRα- and TCRβ-chain sequences (1). For the past two decades, much of the work in the field has focused on iNKT cells because of the ability of α-galactosylceramide (α-GalCer)-loaded CD1d tetramers to specifically identify these cells (2).

iNKT cells and dNKT cells are physiologically distinct cell populations. Not only do these two cell populations recognize different lipids bound within CD1d molecules, even the topology of how their TCRs recognize the CD1d–lipid Ag complex can be clearly different (3). For iNKT cells, the orientation between the iNKT TCR and the CD1d–α-GalCer complex is parallel and focused over the F′ pocket of CD1d, biasing the majority of the TCR–CD1d interaction toward the invariant TCRα, with CDR1α and CDR3α accounting for all interactions with the α-GalCer Ag headgroup (4, 5). In contrast, two recent studies described the crystal structures of dNKT (clone XV19)-derived TCRs in ternary complexes with the glycolipids sulfatide or lysosulfatide bound to CD1d (6, 7). They revealed that these TCRs bound in a manner more analogous to MHC-restricted TCRs, with an orthogonal orientation in which both TCRα's and TCRβ's CDR1 and CDR2

*Division of Rheumatology, Immunology, and Allergy, Department of Medicine, Brigham and Women's Hospital, Harvard Medical School, Boston, MA 02115; [†]Department of Microbiology and Immunology, Peter Doherty Institute for Infection and Immunity, University of Melbourne, Parkville, Victoria 3010, Australia; [‡]Australian Research Council Centre of Excellence in Advanced Molecular Imaging at University of Melbourne, Parkville, Victoria 3010, Australia; [§]Department of Biochemistry and Molecular Biology, School of Biomedical Sciences, Monash University, Clayton, Victoria 3800, Australia; [¶]Australian Research Council Centre of Excellence in Advanced Molecular Imaging, Monash University, Clayton, Victoria 3800, Australia; [‖]School of Biosciences, University of Birmingham, Birmingham B15 2TT, United Kingdom; [#]Division of Endocrinology, Metabolism, and Lipid Research, Washington University, St. Louis, MO 63110; **Department of Pathology, Brigham and Women's Hospital, Harvard Medical School, Boston, MA 02115; and [††]Institute of Infection and Immunity, Cardiff University School of Medicine, Heath Park, Cardiff CF14 4XN, United Kingdom

Received for publication May 4, 2015. Accepted for publication July 10, 2015.

This work was supported by National Institutes of Health Grants 5R01AI063428-09 and 5T32AR007530-30 (to the Brenner Laboratory), National Health and Medical Research Council of Australia Grants 1021972 and 1013667 (to the Godfrey Laboratory), and Australian Research Council Grant CE140100011. G.S.B. acknowledges support in the form of a Personal Research Chair from Mr. James Bardrick and the Medical Research Council (MR/K012118/1). F.-F.H. was supported by Washington University Mass Spectrometry Resource Grants P41-GM103422, P60-DK-20579, and P30-DK56341. M.B.B. was supported by National Institutes of Health Grants 5K08AI077795 and 1R21AI103616. C.F.A. was supported by Fundacao para a Ciência e Tecnologia International PhD Programme SFRH/BD/74906/2010 from Ministério da Educação e Ciência, Portugal. D.I.G. was supported by National Health and Medical Research Council of Australia Senior Principal Research Fellowship 1020770. J.R. was supported by a National Health and Medical Research Council of Australia Fellowship, the National Health and Medical Research Council of Australia, and the Australian Research Council. A.P.U. was supported by Australian Research Council Future Fellowship FT140100278.

Address correspondence and reprint requests to Dr. Michael B. Brenner, Division of Rheumatology, Immunology, and Allergy, Brigham and Women's Hospital, Department of Medicine, Harvard Medical School, Smith Building, Room 552, One Jimmy Fund Way, Boston, MA 02115. E-mail address: mbrenner@research.bwh.harvard.edu

The online version of this article contains supplemental material.

Abbreviations used in this article: AMPP, *N*-(4-aminomethylphenyl) pyridinium; CD1d-bio, biotinylated mouse CD1d; C:M, chloroform:methanol; DGDC-Sp, DGDG from *S. pneumoniae*; DGDG, digalactosyldiacylglycerol; dNKT, diverse/type II NKT; DPG, diphosphatidylglycerol; ELSD, evaporative light scattering detector; FSC, forward scatter; α-GalCer, α-galactosylceramide; GC-MS, gas chromatography–mass spectrometry; GD3, disialoganglioside GD3; iNKT, semi-invariant/type I NKT; KO, knockout; LC-MS, liquid chromatography–mass spectrometry; LSU, light scattering unit; MFI, mean fluorescence intensity; MPA, molybdophosphoric acid; MS/MS, tandem mass spectrometry; phosphatidylglycerol-Cg, phosphatidylglycerol from *C. glutamicum*; RAW, RAW 264.7; RAW-CD1d, RAW cell stably transfected with CD1d; RU, response unit; SPR, surface plasmon resonance; TBS-Tyl, TBS (pH 8) supplemented with 0.05% tyloxapol; TLC, thin layer chromatography.

loops bind, perched over the A′ pocket, to CD1d, and the CDR3β loop provided the major contact with the bound sulfatide headgroup. Whether this is typical of all dNKT TCR–CD1d–Ag interactions remains to be determined, although recent crystallographic studies of a human γδ TCR, and a hybrid δαβ TCR, interacting with lipid Ags α-GalCer and sulfatide, presented by CD1d, also showed orthogonal docking over the A′ pocket of CD1d (7–9). The fact that dNKT TCRs use diverse TCRα- and TCRβ-chains, and that the XV19 CD1d–dNKT TCR structural studies revealed that the variable CDR3 loops can dominate in lipid Ag recognition, suggests that dNKT cells may possess the capacity to recognize a great range of self and foreign lipid Ags.

One of the key distinguishing features of dNKT cells is that unlike iNKT cells, they do not respond to α-GalCer and, therefore, are not identified by CD1d–α-GalCer tetramers. With the finding that dNKT cells may be present in humans at higher levels than iNKT cells, there is great interest in identifying physiologically relevant lipid Ags for dNKT cells (6, 10). Many of the identified dNKT cell lipid Ags were identified or confirmed by screening a panel of dNKT cell hybridomas. Using these T–T hybridomas, several endogenous mammalian lipid Ags (e.g., sulfatide, phosphatidylglycerol, lysophosphatidylcholine, lysophosphatidylethanolamine, and diphosphatidylglycerol) were confirmed as dNKT cell Ags (11–18).

With the notable exceptions of sulfatide-reactive and Gaucher lipid–reactive dNKT cells (12, 19), no other dNKT cell population has been directly identified in vivo because of the failure of tetramers to bind. Instead, the role of dNKT cells was inferred indirectly by comparing mice lacking iNKT cells (Jα18-knockout [KO] mice) with mice lacking both dNKT and iNKT cells (CD1d-KO mice) (20, 21). Studies with these KO mice demonstrated a protective role for dNKT cells in a variety of pathogenic states, including type 1 diabetes, Con A–induced hepatitis, and murine infection with *Schistosoma mansoni* or *Listeria monocytogenes* (1, 10). However, these studies were confounded by the fact that Jα18-KO mice have additional TCR Jα defects, resulting in a limited TCRα repertoire that has only recently been appreciated (22).

Previously, we identified the first microbial dNKT cell lipid Ags (13). Using dNKT cell hybridomas, we found that phosphatidylglycerol and diphosphatidylglycerol (DPG) derived from *Mycobacterium tuberculosis*, the related *Corynebacterium glutamicum*, and mammalian phosphatidylglycerol are Ags for a subset of dNKT cells. The microbe-derived phosphatidylglycerols and DPGs contained the same headgroup as their mammalian counterparts but differed in their dominant fatty acid tail structure. The *Corynebacterium*-derived phosphatidylglycerol/DPG variants were weak Ags and equivalent to the similarly weak mammalian phosphatidylglycerol/DPG with regard to their ability to activate dNKT cells. We reasoned that microbial lipid Ags for dNKTs that are distinctly more active than mammalian phosphatidylglycerol might exist. Therefore, we designed an independent and unbiased search for potential dNKT lipid Ags from other microbes, such as *L. monocytogenes*.

Listeria is a Gram-positive facultative intracellular bacterium that infects and resides within the cytosol of macrophages, dendritic cells, hepatocytes, and epithelial cells (23–25). This pathogen is a common food contaminant and causes significant mortality in immunocompromised individuals and spontaneous abortions in pregnant women (26). There are three key reasons for investigating *Listeria* for lipid Ags. First, as an intracellular pathogen the *Listeria*-derived lipids would be likely to access the intracellular CD1d Ag-presentation system in vivo. Second, data from the comparison of bacterial burdens in Jα18-KO mice and CD1d-KO mice suggest a role for dNKT cells in clearing this pathogen (27, 28). Third, *Listeria* has been subjected to lipidomics analysis, whereby Fischer and Leopold (29) identified many unique *Listeria* lipids that do not have mammalian homologs and, thus, might be recognized as foreign. Furthermore, our analysis of the lipidomics data revealed that a number of these lipids are capable of binding to CD1d, making them potential dNKT lipid Ags.

In this study, we used a panel of iNKT and dNKT hybridomas to screen fractionated *Listeria* lipids for CD1d-restricted Ags. Interestingly, this unbiased screen revealed reactivity in some of the same chemical classes of lipids identified previously, such as phosphatidylglycerol, but with critically important differences. *Listeria*-derived phosphatidylglycerol and DPG differed significantly in their fatty acid architecture compared with the mammalian/*Corynebacterium* variants. Importantly, *Listeria*-derived phosphatidylglycerol is a strikingly more potent Ag for dNKT cells. By performing lipid Ag CD1d-binding assays and tetramer staining, we provide insights into the structural basis for the high potency of microbial compared with mammalian lipid Ags that share identical lipid headgroups.

Materials and Methods

Growth and lipid extraction of L. monocytogenes

Wild-type *L. monocytogenes* (strain 10403S; a gift from H. Shen, University of Pennsylvania) was grown in brain-heart infusion broth (BD Biosciences) supplemented with 200 μg/ml streptomycin (Sigma-Aldrich) overnight to stationary phase at 37˚C and 225 rpm. The following day, flasks containing prewarmed brain-heart infusion broth (BD Biosciences) supplemented with 200 μg/ml streptomycin were inoculated at ∼1:420 v/v and grown until mid-log phase ($OD_{600} \geq 0.4$). Once at mid-log phase, bacteria were pelleted by centrifugation, washed with PBS, and lyophilized. After up to 48 h of lyophilization, *Listeria* pellets were processed for extraction of crude polar lipids, as previously described (30). Once isolated, lipids were weighed, resuspended in 2:1 v/v chloroform:methanol (C:M), and stored in 15-ml glass tubes at −20˚C until used.

Cell lines

The following mouse NKT hybridomas were tested for reactivity against *Listeria* lipids: 24.9, DN32, 14S.6, 14S.10, 14S.15, 431.A11, TBA7, VII68, VIII24.1.D, and XV19.2 (31–34). The hybridomas not generated in the Brenner laboratory were kindly provided by S. Cardell (Göteborgs Universitet) and A. Bendelac (University of Chicago). Hybridoma cells were maintained in NKT growth media (RPMI 1640 [Life Technologies] supplemented with 10% v/v FBS [Gemini], 10 mM HEPES [Life Technologies], 2 mM L-glutamine [Life Technologies], 100 U/ml penicillin [Life Technologies], 100 μg/ml streptomycin [Life Technologies], and 55 nM 2-ME [Life Technologies]). RAW 264.7 (RAW) and RAW cells stably transfected with mouse CD1d (RAW-CD1d) were maintained in Complete DMEM (DMEM supplemented with 10% v/v FBS [Gemini], 2 mM L-glutamine [Life Technologies], 100 U/ml penicillin [Life Technologies], 100 μg/ml streptomycin [Life Technologies]). When hybridomas were cocultured with RAW or RAW-CD1d cells or with plate-bound rCD1d, cells were incubated overnight in Complete RPMI (RPMI 1640 [Life Technologies] supplemented with 10% v/v FBS [Gemini], 2 mM L-glutamine [Life Technologies], 100 U/ml penicillin [Life Technologies], 100 μg/ml streptomycin [Life Technologies]). For tetramer and dextramer experiments, the TCR-deficient T cell hybridoma BW58 (35) was stably transfected with CD3, TCRα, and TCRβ from one of four hybridomas (Vβ8.2 [an iNKT cell hybridoma], TBA7 [$TBA7^{high}$], 14S.6, or XV19). BW58- and TCR-transfected clones were maintained in DMEM-NKT media (DMEM [Life Technologies] supplemented with 10% v/v FBS [Gemini], 15 mM HEPES [Life Technologies], 2 mM L-glutamine [Life Technologies], 100 U/ml penicillin [Life Technologies], 100 μg/ml streptomycin [Life Technologies], 55 nM 2-ME [Life Technologies], 1 mM sodium pyruvate [Life Technologies], and 1× nonessential amino acids [Life Technologies]). All cells were maintained in 37˚C incubators at 5% (RPMI media) or 10% (DMEM media) CO_2.

Liquid chromatography–mass spectrometry fractionation of polar Listeria *lipids*

Preparative HPLC experiments were carried out using a custom Waters (Milford, MA) Autopurification HPLC system comprising a Waters 2767 one-bed injection-collection sample manager, a 2545 quaternary gradient

module that can pump up to 150 ml/min, a system fluidic organizer coupled to a single-quadrupole Waters 3100 Mass Detector equipped with Z Spray API ion source, a Waters 2424 evaporative light scattering detector (ELSD), and a Waters 2998 photodiode array detector. In addition, during preparative mode, the system is coupled to two Waters 515 HPLC pumps used for make-up liquid delivery, as well as a 1000:1 splitter that can tolerate a flow rate of 8–30 ml/min. During fractionation, 99.9% of the lipid is sent to a fraction collector for use in future bioassays. A small percentage (0.1%) of the polar lipid is sent to the detectors to identify the lipid-containing fractions to help with fractionation. The entire system was controlled by MassLynx 4.1 software. Chromatographic analyses and separation of crude polar extracts were performed based on the eluent method on a chemically bonded polyvinyl alcohol-silica stationary phase (36). The total liquid chromatography–mass spectrometry (LC-MS) run was pooled into 19 fractions using time and an ELSD to designate fractions. Pooled fractions were weighed, resuspended in 2:1 C:M, and stored at −20˚C until ready for use.

Analytical and preparative thin layer chromatography

For analytical thin layer chromatography (TLC), lipids were spotted onto aluminum-backed silica TLC plates (EMD Chemicals) and dried under low pressure. Next, lipids were resolved in a solvent system designed for the optimal separation of phospholipids (chloroform:acetic acid:methanol: water at a ratio of 40:25:3:6 v/v/v/v). Plates were dried under low pressure, cut (if appropriate), and sprayed with one of four TLC stains: Dittmer-Lester reagent (phosphate stain), α-naphthol (sugar stain), molybdophosphoric acid (MPA; a general stain), or ninhydrin (an amino group stain) (29, 30). Charring of sugar-stained, MPA-stained, and amino group–stained plates was used to develop those plates. Preparative TLCs were performed by first spotting the lipid across the origin of a plastic-backed TLC plate (EMD Chemicals). The plates were then dried under low pressure, resolved in the 40:25:3:6 system, and dried as above. Next, a small segment of the TLC plate was cut off for staining with one of the above TLC stains, which was used to mark the bands of lipid in the unstained section of the plate. The marked silica regions for each lipid band were scraped off the plastic and moved to 15-ml glass tubes, and the lipid was extracted from the silica with three sequential washes of 2:1 C:M. After drying, lipids were weighed, resuspended in 2:1 C:M, and stored at −20˚C until used. It is critical to note that the amount of TLC purified lipid in the tube cannot be determined solely by measuring weight, because the measured weight includes some transferred silica. When the identity of the purified lipid was unknown (Fig. 3B), lipids were resuspended in 2:1 C:M based on the total weight of the tube and an estimated expected yield. Because the weights for resuspended lipids were approximated, the amount loaded is shown as the fold-dilution of the stock lipid. To determine the relative concentration for identified lipids, concentrations were measured by spotting both the TLC-purified lipid and a relevant standard (*Corynebacterium* phosphatidylglycerol, DPG, or *Streptococcus* digalactosyldiacylglycerol [DGDG]) onto an analytical TLC plate at various concentrations to generate a standard curve. The plates were then dried, resolved with the 40:25:3:6 system, redried, stained with MPA, and charred to develop. The plates were scanned at ≥ 600 dpi, densitometry was performed with ImageJ software (National Institutes of Health), and quantification was determined by comparison with known standards.

Measuring reactivity to lipids by ELISA

RAW or RAW-CD1d cells were resuspended in Complete RPMI, and 5×10^4 cells were plated onto 96-well round-bottom plates (Falcon). Lipids were transferred to 10-ml conical glass tubes (Kimble Chase), dried in a Genevac EZ-2 personal evaporator, resuspended in Complete RPMI, serially diluted, and added to each well as appropriate. No-lipid control wells were given Complete RPMI from 10-ml glass tubes dried with an equivalent volume of the lipid vehicle (2:1 C:M). After a preincubation at 37˚C and 5% CO_2 for ≥30 min, 5×10^4 hybridoma cells were added to each well and cultured for 16–18 h. Supernatants were removed and analyzed for the presence of IL-2 by sandwich ELISA with matched anti-mouse IL-2 Ab pairs (BD Pharmingen). IL-2 protein for ELISA standards was from R&D Systems.

Plate-bound presentation of lipids in CD1d

Lipids or 2:1 C:M vehicle was dried in a Genevac EZ-2 personal evaporator and resuspended in 50 mM (pH 6) citrate buffer supplemented with 0.25% CHAPS (Sigma-Aldrich). The lipid was then mixed with biotinylated CD1d (provided by the National Institutes of Health Tetramer Facility) that also was diluted into 50 mM (pH 6) citrate buffer supplemented with 0.25% CHAPS at a 20:1 w/w ratio in glass HPLC insert tubes (Supelco). Lipids were bound to CD1d for 24–48 h, after which the pH was adjusted to 7.4 with 1 M Tris (pH 9). Finally, PBS was added to double the initial loading volume before storage at 4˚C until use. For binding CD1d onto plates, 0.05, 0.2, or 0.25 μg CD1d was added per well of a streptavidin-coated plate (Thermo Scientific Pierce) for 1 h at room temperature. Plates were washed extensively with sterile PBS before the addition of 5×10^4 hybridoma cells/well in Complete RPMI. After 16–18 h at 37˚C and 5% CO_2, supernatants were collected, and IL-2 was analyzed by ELISA.

Tetramers, dextramers, and flow cytometry

Biotinylated mouse CD1d (provided by the National Institutes of Health Tetramer Facility) was diluted into TBS (pH 8) to 0.4 mg/ml, and lipids were dried as above and then resuspended in TBS (pH 8) supplemented with 0.05% tyloxapol (TBS-Tyl; Acros Organics) at 1 mg/ml. Lipids or TBS-Tyl vehicle (mock) was mixed with CD1d in HPLC insert tubes at a molar ratio of 35:1 lipid/CD1d molecules. After a 20–24-h incubation at 37˚C, CD1d was formed into tetramers by incubation with streptavidin-allophycocyanin (Invitrogen) or diluted with PBS to 0.1 mg/ml CD1d and stored at 4˚C for future loading into dextramers. Dextramer-allophycocyanin backbone (a gift from Immudex, Copenhagen, Denmark) was mixed with CD1d at a ratio of 4 CD1d molecules:1 streptavidin binding site on the Dextramer backbone ≥30 min before use.

For flow cytometry, 5×10^4 hybridoma cells/well were preincubated with Brilliant Violet 421–labeled PBS-57 (an α-GalCer analog) CD1d tetramers (provided by the NIH Tetramer Facility) and then stained with APC-labeled mock or loaded tetramers (0.8 μg CD1d/well) or dextramers (3 μl Dextramer-allophycocyanin backbone plus 1.15 μg CD1d/well). Finally, cells were stained with PE-labeled anti–TCR-β (clone H57-597; BioLegend) and analyzed on a BD FACSCanto II flow cytometer. Data were analyzed with FlowJo (TreeStar). For analysis, samples were gated first by forward scatter (FSC)-A and side scatter-A to identify live cells, followed by singlet gating (FSC-A by FSC-H). Next, cells were gated for TCR expression. Tetramer or dextramer (mean fluorescence intensity [MFI] of allophycocyanin-A) levels were determined.

Mass spectrometric identification of lipid structure

Both high-resolution (R = 100,000 at m/z 400) and low-energy collision activated dissociation tandem mass spectrometry (MS/MS) were performed as previously described, with the exceptions that samples were dissolved into methanol instead of 2:1 C:M, the automatic gain control of the ion trap was set to 5×10^4, and the electrospray needle was set to 4.0 kV (13). For structural analysis of fatty acids, TLC-purified lipids were treated via alkaline hydrolysis to liberate fatty acids, which were then isolated and derivatized with *N*-(4-aminomethylphenyl) pyridinium (AMPP) and subjected to mass spectrometry, as described (37).

Synthesis of lipid standards

Synthesis of mammalian (18:1/16:0) or *Listeria* (15:0/17:0) phosphatidylglycerols was performed in a stepwise fashion, starting with a glycerol backbone, as described in Supplemental Fig. 3.

Generation of soluble TCR and CD1d

Mouse CD1d/β2m expression vector with a BirA and 6-histidine tag (construct originally provided by Mitchell Kronenberg, La Jolla Institute of Allergy and Immunology) was expressed, purified, and biotinylated in-house, as previously described (38). Soluble mouse TCR production was achieved using chimeric mouse-variable–human-constant domains, as previously described (38). Individual TCR chains were cloned into pET-30 (Novagen) vectors for the TCRβ-chain or pET-28 (Novagen) for the TCRα-chain and expressed in BL-21 *Escherichia coli* (DE3)pLysS. Inclusion body protein preparations were isolated and refolded as previously described (39), with the exception of the addition of 5 M urea into the refold buffer. TCRs were purified by anion-exchange chromatography, immobilized metal-affinity chromatography, and gel filtration. TCR purity was assessed by gel electrophoresis, and predicted mass was confirmed by time-of-flight mass spectrometry. TCR refolding was confirmed by ELISA using an Ab reactive against a conformational epitope for the TCR constant domain (clone 12H8; produced in-house) and anti-Vβ8.1/8.2 (clone KJ16-133; eBioscience).

Disialoganglioside GD3 lipid-displacement assay

Disialoganglioside GD3 (GD3; Matreya #1504) was suspended in TBS-Tyl at 1 mg/ml and mixed at a 3:1 molar ratio with in-house–generated biotinylated mouse CD1d (CD1d-bio) at 1 mg/ml in TBS (pH 8) for 20 h at room temperature. GD3-loaded CD1d-bio was purified by MonoQ anion-

exchange chromatography. *Listeria* phosphatidylglycerol or *Corynebacterium* phosphatidylglycerol, resuspended at 1 mg/ml in TBS-Tyl, was incubated at a 30:1 molar ratio with purified GD3-loaded CD1d-bio. Phosphatidylglycerol-loaded fractions were purified using MonoQ anion-exchange chromatography. These fractions were used in affinity measures with TBA7 by surface plasmon resonance (SPR). Excess lipid and detergent were removed prior to each chromatography run using a PD10 desalting column (Amersham Biosciences).

SPR analysis

SPR experiments were performed at 25˚C on a Biacore 3000 instrument and conducted in HEPES buffered saline (10 mM HEPES [pH 7.4] 150 mM NaCl); 1% BSA was added to prevent any nonspecific binding. Four thousand response units (RU) CD1d-bio loaded with the lipid Ag *Corynebacterium* phosphatidylglycerol or *Listeria* phosphatidylglycerol–LC-MS fraction E were coupled onto the streptavidin sensor chip. An HLA class I molecule was immobilized on one flow cell for reference subtraction. Biotin was injected to block the free streptavidin sites. Nine serial dilutions of TBA7 from 200 to 0.78 μM were passed through as analyte. BIAevaluation software was used for data analysis.

Data presentation and statistical analysis

All IL-2 ELISA graphs, fold-change graphs, and percentage displacement graphs were generated using GraphPad Prism 5.0b. All statistical analyses (one-way ANOVA) were performed with GraphPad Prism 5.0b.

Results

We isolated polar *Listeria* lipids from mid-log phase bacteria cultures and cocultured the crude polar lipid mixture with two iNKT cell hybridomas (Fig. 1A, 1B) and eight dNKT cell hybridomas (Fig. 1C–J). To be considered activated, the following requirements were necessary: a dose response between lipid Ag concentration and hybridoma IL-2 production; IL-2 production when cocultured with lipid Ag, and RAW-CD1d is significantly higher than when cocultured with no exogenously added lipid; and little to no response when cocultured with lipid Ag and untransfected RAW cells. By these requirements, both iNKT cell hybridomas (Fig. 1A, 1B) failed to be activated by crude *Listeria* polar lipids, as also noted by other investigators (31–34, 36, 40). In contrast, six of the eight dNKT cell hybridomas were positively activated by *Listeria* polar lipids in a CD1d-dependent manner. Based on these results, we chose two dNKT hybridomas, 14S.6 and TBA7, which gave strong responses to the polar lipid extract for further study to identify the relevant *Listeria* lipid Ags present in the crude extract.

We fractionated the *Listeria* polar lipid extract by preparative HPLC. This preparative LC-MS system involves the use of three isocratic solvent mixtures on a polyvinyl chloride silica column to facilitate separation of lipids based on headgroup structure. Four detectors are used to reveal lipids, including a UV detector, a single quadrupole mass spectrometer, an ELSD, and a photodiode array detector. We used ELSD (measured in light scattering units [LSU]) and retention time as the criteria for separating the total LC-MS run into 19 fractions, which were tested for biological activity. Although fractions encompassing the whole run were tested for activity, the major antigenic fractions correlated with the presence of detectable LSU signals (Fig. 2A, data not shown). The two major LSU peaks appeared at ~10 min and between 38 and 48 min elution time. The peak at 10 min (Peak 1) was identified by TLC to consist of free fatty acids and roughly equal amounts of 1,2- and 1,3-diacylglycerol (data not shown). The stimulatory Peak 1 fraction was weaker than those collected between 38 and 48 min and was not characterized further. The six LC-MS fractions collected between 38 and 48 min activated the diverse hybridomas 14S.6 and TBA7 in a CD1d-dependent manner (Fig. 2B–E).

The fact that all of these fractions are eluting from the LC-MS column around the same time suggested that they may share common polar headgroups. Further, we noted previously that, in our HPLC system, LSU peaks eluting between 38 and 48 min typically indicate the presence of phospholipids. By analyzing

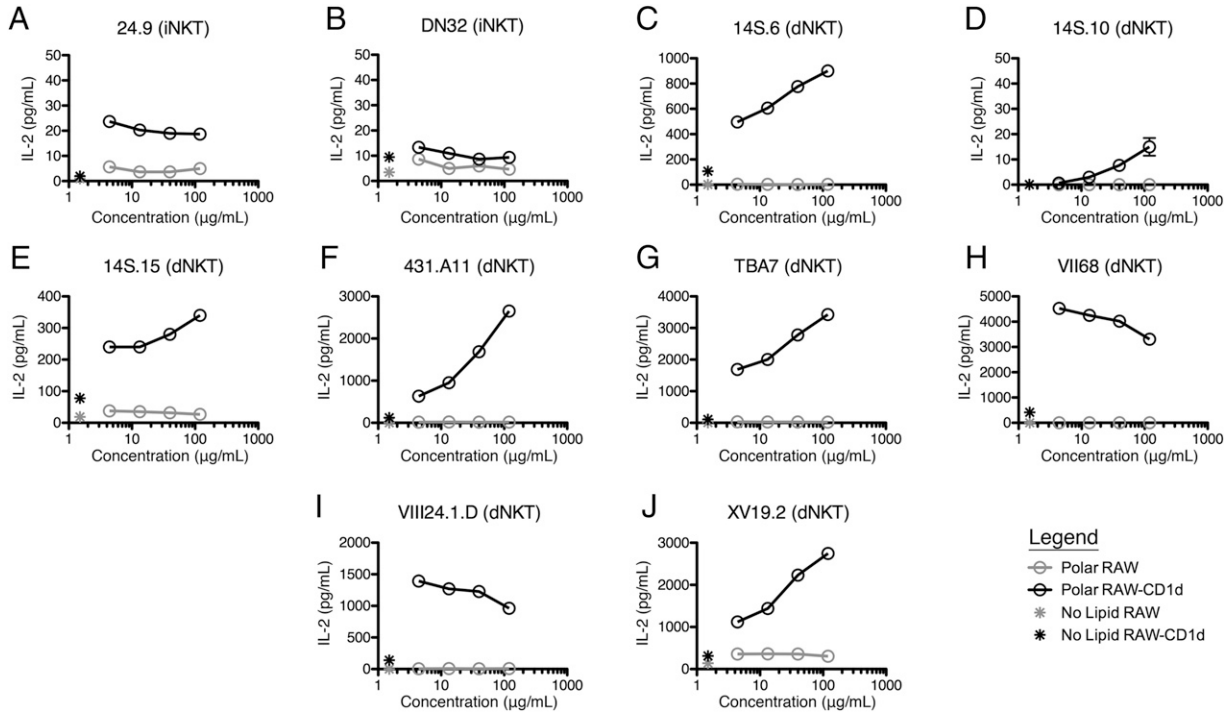

FIGURE 1. *L. monocytogenes* polar lipids activate diverse, but not invariant, NKT hybridomas. Polar lipids derived from the bacterium *L. monocytogenes* were incubated at various concentrations in triplicate with a panel of NKT cell hybridomas in the presence of RAW (gray circles) or RAW-CD1d (black circles) cells. Hybridomas were also cocultured with RAW or RAW-CD1d cells without adding exogenous lipid in duplicate (gray and black asterisks). After 16–18 h of coculture, supernatants were assayed for the presence of IL-2 by ELISA. Each graph shows mean ± SEM and is representative of four (**B**–**D**, **F**, and **G**), three (**A**, **E**, **H** and **J**), or two (**I**) independent experiments.

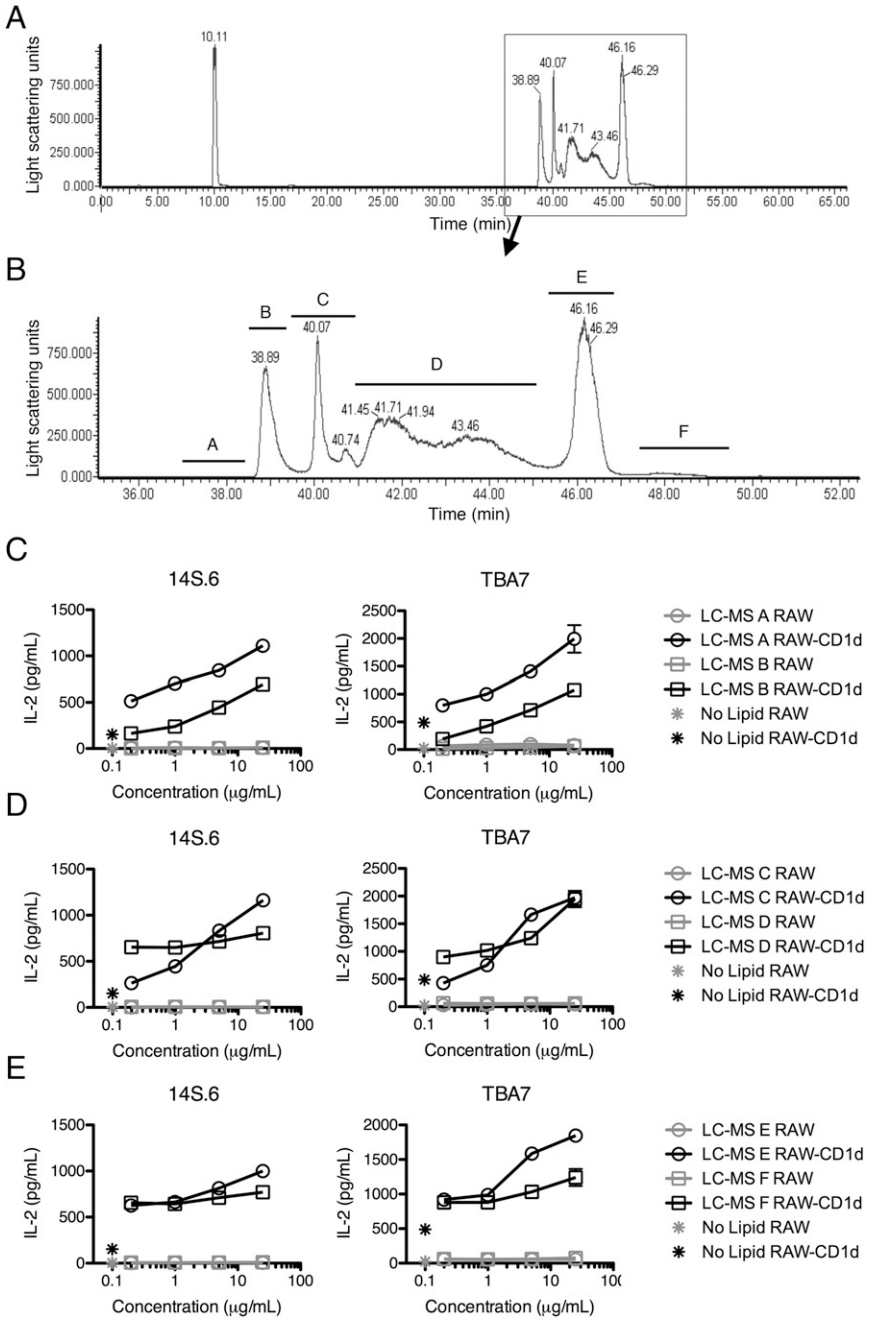

FIGURE 2. LC-MS fractionation of *Listeria* polar lipids. (**A**) *Listeria* polar lipids were subjected to LC-MS fractionation by headgroup. (**B**) *Inset* from (A), highlighting the light-scattering peaks collected for LC-MS fractions A–F. (**C**–**E**) 14S.6 (*left panels*) and TBA7 (*right panels*) hybridomas were incubated with LC-MS fraction A or B (C), fraction C or D (D), or fraction E or F (E) in the presence of RAW cells (gray lines) or RAW-CD1d cells (black lines) in triplicate. Hybridomas were also cocultured with RAW or RAW-CD1d cells without adding exogenous lipid in duplicate (gray and black asterisks). After 16–18 h of coculture, supernatants were assayed for the presence of IL-2 by ELISA. The graphs in (C)–(E) are representative of three independent experiments and show mean ± SEM.

migration on TLC plates in a solvent system designed for resolving phospholipids, we found that fractions A–F included the presence of phosphate-containing lipids that migrated to similar heights, suggesting that they all shared similar structures in different ratios (Supplemental Fig. 1). At the concentrations tested, LC-MS fraction C showed a clear dose response across concentrations and was available in sufficient quantities for further analysis (Fig. 2D). After further separation by TLC, we subjected LC-MS fraction C to a variety of stains (Fig. 3A) (13). Dittmer-Lester (phosphate) stains phosphate-containing molecules a blue color on a white background. α-Naphthol (sugar) stains lipids containing carbohydrate groups a dark purple color. MPA (general) is a general lipid stain that is thought to stain fatty acid tails. Finally, LC-MS fraction C also was stained with ninhydrin (amino), which stains amino groups reddish-pink but also can nonspecifically mark some lipids with a brown color.

Based on these TLC stains, we identified 12 lipid bands from LC-MS fraction C and isolated each by preparative TLC. These bands were tested for activity with hybridoma 14S.6 (Fig. 3B). The top six bands (TLC 1–6), which contained all of the phosphate- or sugar-positive lipid bands, activated hybridoma 14S.6, but the bottom six bands did not. MS/MS on the six active TLC bands identified these as lipid species with glycerol backbones, and each lipid was dominated by fatty acid tails of length 17:0/15:0 in the *sn1* and *sn2* positions, respectively. By MS/MS analysis of the TLC-purified lipids, TLC bands 1–3 consisted of DPG (Fig. 3C), TLC band 4 was identified as phosphatidylglycerol (Fig. 3D), and TLC band 5 was DGDG (Supplemental Fig. 2C). However, further TLC-based analysis of TLC-purified DGDG from *Listeria* determined that this activity was likely due to a comigrating UV light$^+$ molecule. DGDG from either *Streptococcus pneumoniae* or LC-MS fraction B (that did not contain the comigrating UV$^+$ band) was inactive (Supplemental

Fig. 2B). TLC band 6 was not visible by any of the four TLC stains, and MS/MS data were inconclusive. We next generated AMPP derivatives of the fatty acid tails for further analysis of the fatty acid structure by gas chromatography-MS (GC-MS) (37). GC-MS on AMPP derivatives from DPG, phosphatidylglycerol, and DGDG revealed that the fatty acids are predominately anteiso methyl-branched fatty acids (Fig. 3E, 3F), a structure that is not found in mammals (35, 41).

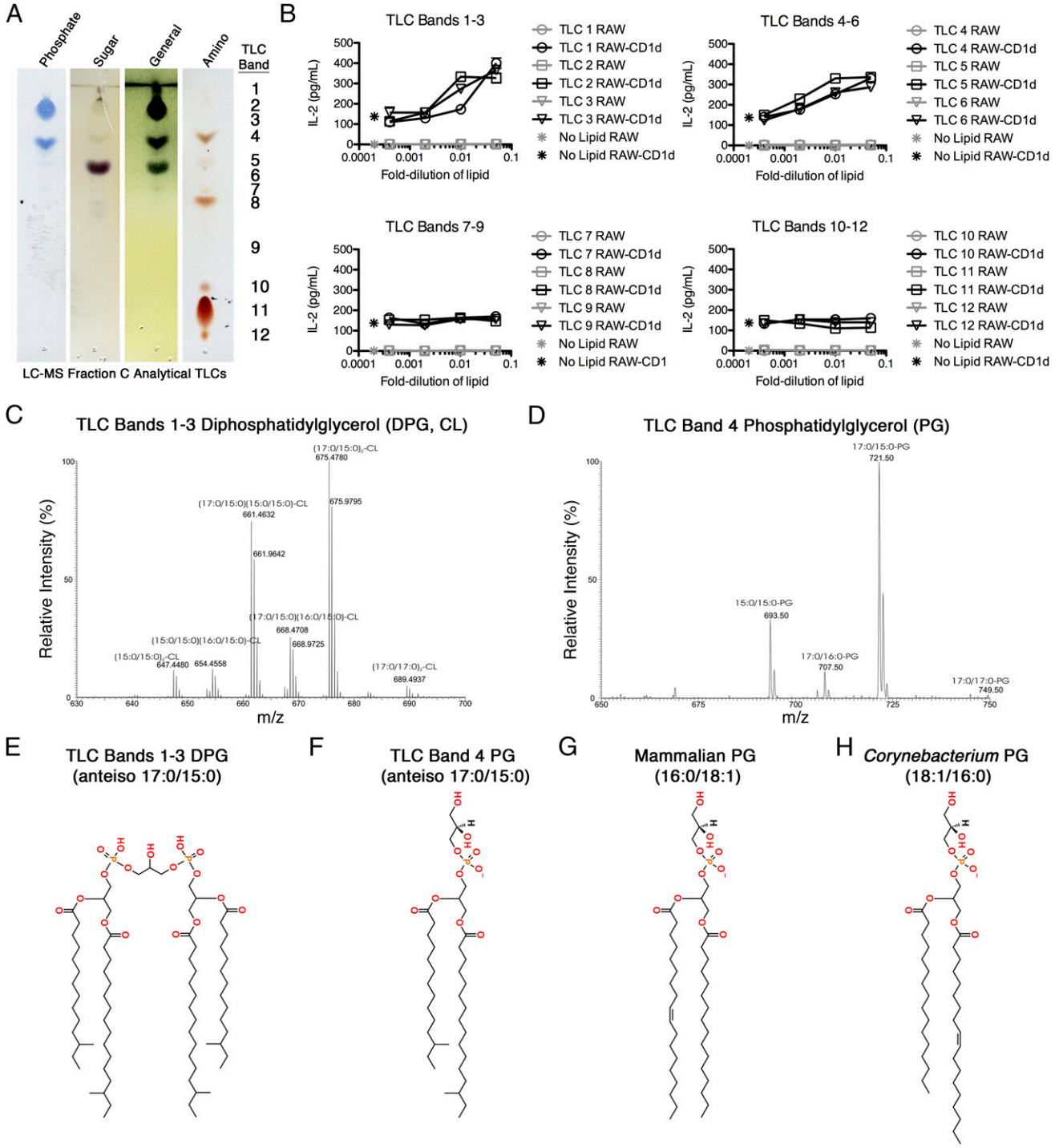

FIGURE 3. TLC purification of LC-MS fraction C identifies six active bands. (**A**) *Listeria* LC-MS fraction C was spotted at 150 μg/spot on a TLC plate and run in the 40:25:3:6 system. The plate was cut into strips, and each strip was stained with one of four stains: Dittmer-Lester reagent (Phosphate; to stain phosphate groups), α-naphthol (Sugar; to stain sugar groups), MPA (General; a general fatty acid tail stain), and ninhydrin (Amino; to stain amino groups). These stains were used to identify 12 lipid bands for extraction. (**B**) TLC plate-eluted lipid bands were incubated with 14S.6 cells and RAW (gray) or RAW-CD1d (black) cells in triplicate. Because of the silica plate extraction, weights of TLC bands reflected both silica and lipid weight. Therefore, the lipid bands were resuspended based on total weight, and fold dilutions of the stock lipids are displayed. IL-2 ELISAs were performed on culture supernatants after 16–18 h of coculture. Data are representative of two independent experiments and show mean ± SEM. Collision MS/MS spectra for TLC bands 1–3 were all identified as DPG (**C**), and TLC band 4 was identified as phosphatidylglycerol (**D**). Structures of the dominant DPG (**E**) and phosphatidylglycerol (**F**) lipids in the TLC bands, with comparison with mammalian (**G**) and *Corynebacterium* (**H**) phosphatidylglycerol, demonstrating the different fatty acid tails found in these species.

LC-MS fractions A–F contain phospholipids that resolve on TLC plates with similar mobilities, suggesting that these fractions contain lipids with the same headgroups (Supplemental Fig. 1). Next, we used TLC to isolate putative DPG and phosphatidylglycerol bands from the other LC-MS fractions that contained enough materials for further study (fractions B–E) and confirmed by MS/MS that these were DPG or phosphatidylglycerol and that the major fatty acid tails were anteiso isomers by GC-MS on AMPP derivatives of the fatty acid tails. In total, we isolated DPGs from LC-MS fractions B–E and phosphatidylglycerols from LC-MS fractions C–E. Although the same lipid was found throughout multiple fractions, we identified differences in the fatty acid substituent compositions. These differences included the presence or absence of plasmenyl phosphatidylglycerol (fatty acids with an *sn1* ether linker and an *sn2* ester linker) (37) and different ratios of phosphatidylglycerol species (e.g., the ratio of 15:0/15:0 to 17:0/16:0 and 17:0/17:0) (Fig. 3D, data not shown).

Recently, we reported that phosphatidylglycerol and DPG were dNKT cell Ags derived from mammals or *C. glutamicum* (13). However, the two species had very similar lipid structures; notably the same dominant fatty acid tails (16:0 and 18:1) were present but opposite in *sn1* and *sn2* orientation (Fig. 3G, 3H). Importantly, when *Corynebacterium* phosphatidylglycerol or DPG was compared with mammalian phosphatidylglycerol or DPG, there was no difference in their potency with regard to the activation of dNKT cells (13). Unlike the previously described phosphatidylglycerol and DPG lipids from mammals, *Listeria* phosphatidylglycerol and DPG have a distinct fatty acid architecture, prompting us to ask whether *Listeria* phosphatidylglycerol and DPG are more or less stimulatory than the corresponding mammalian (or *Corynebacterium*) sources. When comparing the ability to activate hybridomas 14S.6 and TBA7, *Listeria* DPG was an equally potent Ag to *Corynebacterium* DPG (Supplemental Fig. 2A). However, we found that *Listeria*-derived phosphatidylglycerols were strikingly more potent Ags than *Corynebacterium*-derived phosphatidylglycerol, as measured by their ability to activate the dNKT hybridomas at lower lipid concentrations (Fig. 4A). Next, we calculated the *Listeria* phosphatidylglycerol concentration needed to obtain an equivalent level of IL-2 production as the first *Corynebacterium* concentration to be clearly above background levels (Table I). When we calculated the fold change in concentration needed to get the same level of activity, we found that the *Listeria* phosphatidylglycerols were 10–100-fold more potent than *Corynebacterium*-derived phosphatidylglycerol, which is similar in potency to phosphatidylglycerol from mammals (Fig. 4B, Table II).

To confirm these findings, we synthesized the dominant *Listeria* phosphatidylglycerol variant (a17:0/a15:0) and compared its ability to activate TBA7 cells with that of synthetic mammalian phosphatidylglycerol (16:0/18:1). These results supported our previous observations that *Listeria* phosphatidylglycerol was a more potent Ag than mammalian phosphatidylglycerol and had a similar fold difference in activity (~13-fold) to *Listeria* LC-MS fractions C and D phosphatidylglycerols (Fig. 4C).

To determine whether cellular processing of *Listeria* phosphatidylglycerol was required for presentation to dNKT cells, we tested activity using an APC-free system. We loaded the most active *Listeria* phosphatidylglycerol (phosphatidylglycerol–LC-MS fraction E) or the prototypical iNKT cell Ag α-GalCer onto biotinylated CD1d and then bound 0.2 μg of CD1d/well to streptavidin-coated plates. Different NKT hybridomas were incubated with the plate-bound CD1d (Fig. 5A). As expected, α-GalCer–loaded CD1d activated the iNKT DN32 hybridoma but did not activate the dNKT TBA7 hybridoma. Importantly, phosphatidylglycerol–LC-MS fraction E–loaded CD1d activated the dNKT TBA7 hybridoma but not the iNKT DN32 hybridoma. Mock-loaded CD1d did not activate DN32 cells, but it weakly activated TBA7 cells, reflecting the known CD1d autoreactivity seen with many dNKT hybridomas. Next, we determined whether the different antigenic properties of the various phosphatidylglycerols would be reflected in this APC-free system. Indeed, when we loaded *Corynebacterium* phosphatidylglycerol or the various TLC-purified *Listeria* phosphatidylglycerols into plate-bound CD1d, we measured a dose-dependent increase in IL-2 production (Fig. 5B, compare *left* and *right panels*). The amount of IL-2 produced at 0.25 μg CD1d/well (Fig. 5B, *right panel*) closely mimicked the fold difference in activity seen in the system using live RAW-CD1d APCs (Fig. 4B, *right panel*), suggesting that the

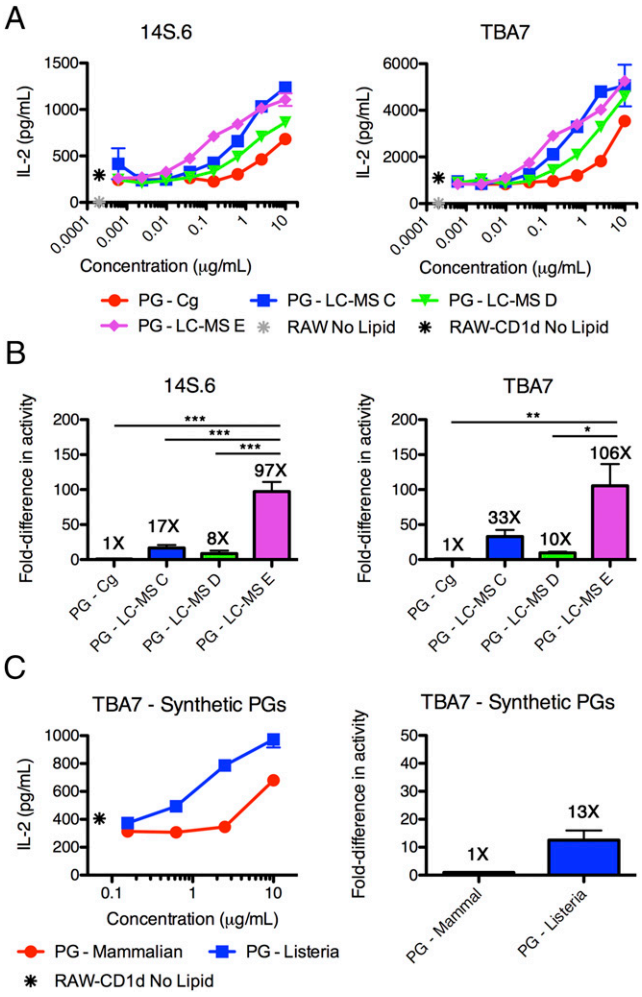

FIGURE 4. *Listeria*-derived phosphatidylglycerols are 10–100-fold more antigenic than *Corynebacterium* or mammalian phosphatidylglycerol. (**A**) Activity of *Listeria* phosphatidylglycerol from fractions C–E was compared with that for phosphatidylglycerol-Cg when cocultured in triplicate with 14S.6 or TBA7 hybridomas in the presence of RAW-CD1d or RAW cells (data not shown). (**B**) The fold difference in concentration required for similar activity to *Corynebacterium* phosphatidylglycerol was calculated. (**C**) Synthetic *Listeria* and mammalian phosphatidylglycerols were assayed for activity, as in (A). The fold difference in concentration required for similar activity to synthetic mammalian phosphatidylglycerol was assayed. Data in (A) are representative of three independent experiments, data in (B) are a combination of three experiments, and data in (C) are representative (*left panel*) or a combination (*right panel*) of two independent experiments. $*p < 0.05$, $**p < 0.01$, $***p < 0.05$, one-way ANOVA. All graphs are presented as mean ± SEM.

Table I. Concentration of *Listeria* phosphatidylglycerols for equivalent activity to *Corynebacterium* phosphatidylglycerol

Replicate	*Corynebacterium*	LC-MS Fraction C	LC-MS Fraction D	LC-MS Fraction E
		14S.6		
1	2.5	0.1	0.15	0.03
2	2.5	0.2	0.8	0.02
3	2.5	0.2	0.4	0.03
		TBA7		
1	10	0.2	1.0	0.06
2	10	0.6	1.5	0.15
3	2.5	0.08	0.2	0.03

All data are μg/ml.

Table II. Replicates for the fold difference in the activity of phosphatidylglycerol

Replicate	*Corynebacterium*	LC-MS Fraction C	LC-MS Fraction D	LC-MS Fraction E
		14S.6		
1	1	25	16.7	83.3
2	1	12.5	3.1	125
3	1	12.5	5.6	83.3
Average	1	16.7	8.4	97.2
		TBA7		
1	1	50	10	166.7
2	1	16.7	6.7	66.7
3	1	16.7	12.5	83.3
Average	1	32.6	9.7	105.6

difference in activity is not due to processing of the LC-MS fractions within RAW-CD1d cells.

These results prompted us to determine whether *Listeria* phosphatidylglycerol was an Ag for the other six dNKT hybridomas. We performed APC-containing (RAW-CD1d cells) and APC-free (plate-bound CD1d) experiments to determine reactivity to *Listeria* phosphatidylglycerol–LC-MS fraction E (Table III). In the APC-free system, three of the hybridomas (14S.6, 14S.10, and TBA7) were reactive to *Listeria* phosphatidylglycerol. These results match what we (13) found for *Corynebacterium* phosphatidylglycerol. In the APC-containing system, an additional two dNKT hybridomas (VII68 and VIII24.1.D) were activated by *Listeria* phosphatidylglycerol. Because we generally found that the plate-bound CD1d system is less sensitive for weak Ags than the APC-containing system, this likely reflects a low-affinity reactivity for *Listeria* phosphatidylglycerol by these two hybridomas.

The high activity of *Listeria* phosphatidylglycerol in the CD1d plate-bound assay compared with other established phosphatidylglycerol sources prompted us to determine whether *Listeria* phosphatidylglycerol-loaded CD1d tetramers would bind to TBA7 cells. In the CD1d plate-bound assay, excess detergent and lipid are washed away before adding hybridoma cells to the wells. To minimize excess detergent and lipid in the tetramer preparations, we first optimized the system by modifying our lipid-loading protocol. In addition, we generated hybridoma cell lines that expressed high levels of TCR. The TCR^{-} immortalized T cell line BW58 was transfected with CD3 and the TBA7 TCR ($TBA7^{high}$) or a typical iNKT cell TCR (Vβ8.2) (35). As expected, CD1d tetramers loaded with PBS-57 (a synthetic α-GalCer analog) stained Vβ8.2 cells but not $TBA7^{high}$ cells (data not shown). Further, *Listeria* phosphatidylglycerol-loaded CD1d tetramers did not bind to Vβ8.2 cells (Fig. 5C), the parent BW58 hybridoma cells (data not shown), or BW58 cells transfected with the phosphatidylglycerol-nonreactive dNKT XV19 hybridoma cell TCR (data not shown). In contrast, we found that tetramers loaded with *Listeria* phosphatidylglycerol–LC-MS fraction E stained $TBA7^{high}$ cells, whereas mock-loaded CD1d tetramer or tetramers made of CD1d loaded with the irrelevant lipid DGDG from *S. pneumoniae* (DGDG-Sp) bound only at background levels (Fig. 5C, *left panels*). Together, these functional and tetramer-staining experiments demonstrate that *Listeria* phosphatidylglycerol-loaded CD1d is a cognate Ag for the dNKT TBA7 TCR.

Listeria phosphatidylglycerol–LC-MS fraction E–loaded tetramers gave a signal that was ∼2-fold higher than vehicle-loaded tetramers (Fig. 5C, *right panels*). We next attempted to increase the positive–negative signal separation using dextramer technology. Dextramers are dextran backbones containing multiple fluorophore and streptavidin binding sites/molecule (42). Because they contain 12–24 Ag-presenting molecules/dextramer backbone, they are useful for identifying rare primary T cell populations because of their increased TCR avidity and fluorescence compared with tetramers. Indeed, Kasmar et al. (43) successfully used CD1a dextramers to identify dideoxymycobactin-restricted T cells ex vivo from human PBMCs. We generated mock-loaded CD1d dextramers along with *Listeria* phosphatidylglycerol–LC-MS fraction E–, phosphatidylglycerol from *C. glutamicum* (phosphatidylglycerol-Cg), or DGDG-Sp–loaded CD1d dextramers and used them to stain dNKT $TBA7^{high}$ BW58 cells transfected with the 14S.6 TCR ($14S.6^{high}$), as well as iNKT Vβ8.2 cells (Fig. 5D, *left panel*, data not shown). We found that phosphatidylglycerol LC-MS fraction E–loaded CD1d dextramers specifically bound to $TBA7^{high}$ cells and gave a signal that was ∼8-fold higher than for vehicle-loaded CD1d dextramers (Fig. 5D, *right panel*). The phosphatidylglycerol LC-MS fraction E–loaded CD1d dextramers did not bind to $14S.6^{high}$ cells (data not shown), suggesting that the 14S.6 TCR affinity for this complex is very low. Finally, we also tested the ability of the less active phosphatidylglycerol from *Corynebacterium* to identify TBA7 TCR-expressing T cells with this newly optimized system. Phosphatidylglycerol-Cg–loaded CD1d dextramers also consistently stained the $TBA7^{high}$ cells, albeit to a much lower degree than did the *Listeria* phosphatidylglycerol–LC-MS fraction E–loaded dextramers; however, the difference did not reach statistical significance (∼1.5-fold higher MFI than mock loaded).

Previous studies on iNKT cell Ags demonstrated that alterations in the fatty acid tails of lipids can dramatically alter their activity, either by modulating their binding to CD1d or by indirectly affecting iNKT TCR recognition (44–46). *Listeria* phosphatidylglycerols are dominated by short chain lengths and fully saturated anteiso methyl-branched fatty acids. In contrast, the less antigenic mammalian or *Corynebacterium* phosphatidylglycerol have longer acyl chains, are unsaturated, and lack anteiso branches. These differences in fatty acid tail composition could alter how well the lipid binds into CD1d, alter the orientation of the phosphatidylglycerol headgroup into a more favorable position for TCR binding, or alter CD1d conformation that subsequently impacts on TCR binding. To test whether the more potent *Listeria* phosphatidylglycerol–LC-MS fraction E loads into CD1d more efficiently than *Corynebacterium* phosphatidylglycerol, we performed a GD3 lipid-displacement assay. GD3 is a negatively charged lipid with a large sugar-based headgroup that can be displaced from CD1d by other lipids. We loaded CD1d with GD3, purified the GD3-loaded CD1d complexes by MonoQ anion-exchange chromatography, and measured the ability of *Listeria* or *Corynebacterium*

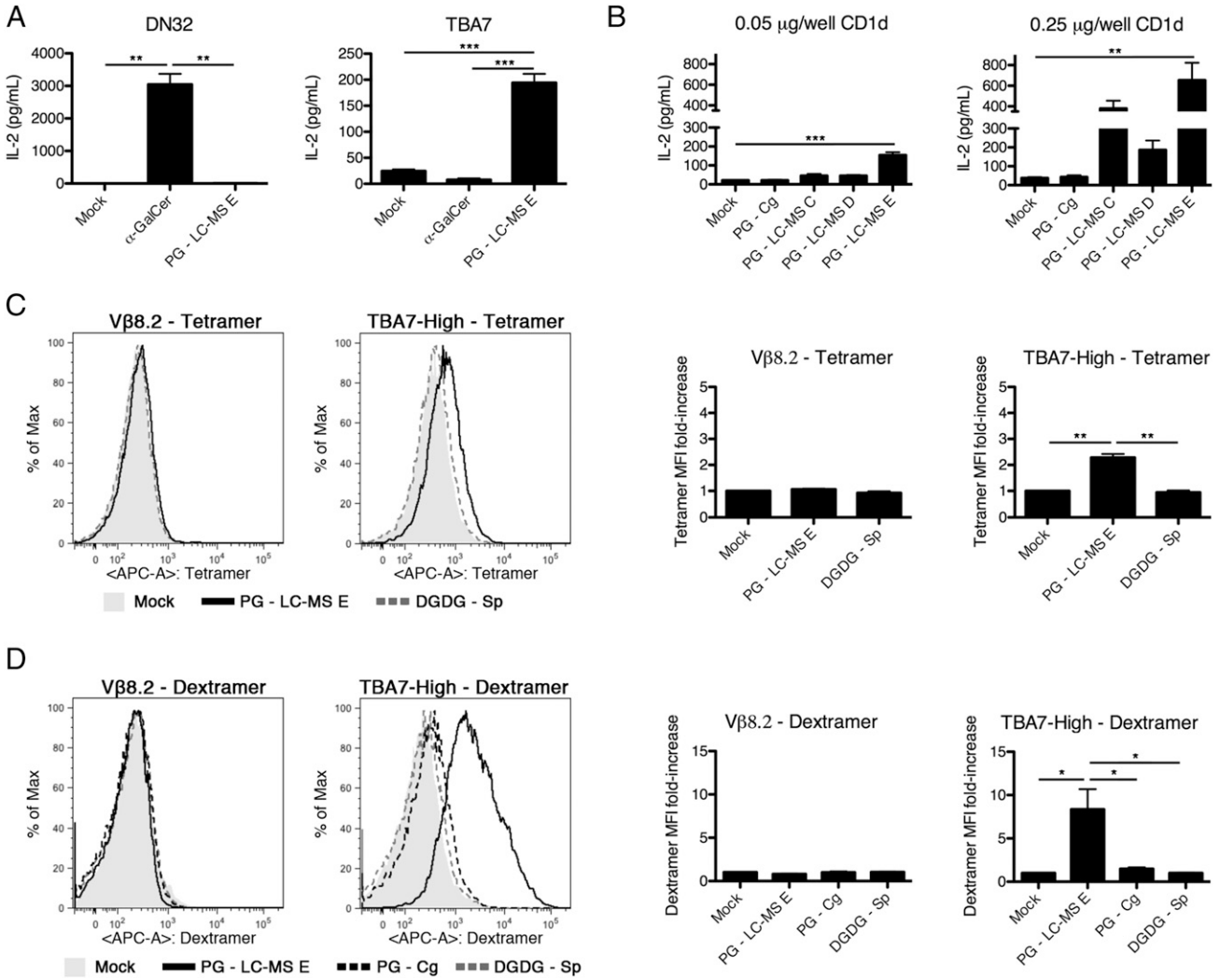

FIGURE 5. TBA7 hybridoma cells recognize *Listeria*-derived phosphatidylglycerols in cell-free systems. (**A**) Biotinylated murine CD1d molecules were mock loaded, loaded with α-GalCer, or loaded with phosphatidylglycerol–LC-MS fraction E. The loaded CD1d molecules were bound to streptavidin-coated plates at 0.2 μg CD1d/well and washed before adding either DN32 or TBA7 hybridomas overnight. The next day, supernatants were analyzed for production of IL-2 by ELISA. (**B**) CD1d molecules that were mock loaded or loaded with various phosphatidylglycerols were bound to streptavidin-coated plates at 0.05 or 0.25 μg CD1d/well and incubated overnight with TBA7 hybridomas. The next day, supernatants were analyzed for production of IL-2 by ELISA. (**C**) TBA7^{high} or Vβ8.2 (iNKT) hybridoma cells were stained with PBS-57 (an α-GalCer analog)-loaded CD1d tetramer at room temperature, followed by staining with mock- or lipid-loaded CD1d tetramers at 37°C. Finally, cells were stained with an anti-TCRβ mAb, washed, and analyzed by flow cytometry. Line graphs show examples of staining patterns with different CD1d tetramers (*left panels*). Bar graphs show fold increase in MFI compared with the mock-loaded CD1d MFI (*right panels*). (**D**) TBA7^{high} or Vβ8.2 TCR-transduced cells were stained with PBS-57–loaded CD1d tetramer, followed by staining with mock- or lipid-loaded CD1d dextramers. After staining with an anti-TCRβ mAb, cells were analyzed by flow cytometry. Line graphs show examples of staining patterns with different CD1d dextramers (*left panels*). Bar graphs show fold increase in MFI compared with the mock-loaded CD1d MFI. Data in (A) and (B) are representative of three independent experiments, with each independent experiment consisting of three technical replicates. Data in (C) and (D) are representative graphs (*left panels*) or combinations (*right panels*) of two independent experiments. The graphs in (A), (B), (C, *right panels*), and (D, *right panels*) are presented as mean ± SEM. $*p < 0.05$, $**p < 0.01$, $***p < 0.001$, one-way ANOVA.

phosphatidylglycerol to displace GD3, which results in earlier elution relative to the CD1d–GD3 complex. We found that *Listeria* phosphatidylglycerol–LC-MS fraction E displaced ~2-fold more GD3 than did *Corynebacterium* phosphatidylglycerol under the same conditions (35% versus 19% loaded, Fig. 6B).

We next used SPR to determine whether the TBA7 TCR affinity for *Listeria* phosphatidylglycerol–LC-MS fraction E differed from that of *Corynebacterium* phosphatidylglycerol. CD1d was loaded with *Listeria* phosphatidylglycerol or *Corynebacterium* phosphatidylglycerol using the GD3-displacement approach described above to ensure optimal loading. CD1d with endogenous lipid Ag was used as a control. These preparations were immobilized to the streptavidin SPR chips via their biotin tags. Purified and soluble TBA7 TCR was then passed over CD1d-Ag, and the binding affinity was measured (in RU). The TCR affinity for *Listeria* phosphatidylglycerol–LC-MS fraction E–loaded CD1d (K_D = 71 μM) was similar to CD1d loaded with *Corynebacterium* phosphatidylglycerol (K_D = 94 μM) (Fig. 6C, 6D). For comparison, these affinities are lower than the previously published TCR affinities for the dNKT hybridoma XV19 TCR binding to sulfatide + CD1d (K_D = 24 μM) or the nanomolar iNKT TCR affinity observed for α-GalCer–loaded CD1d (K_D = 0.07 μM) (6, 38). Accordingly, our data suggest that the increased potency of *Listeria* phosphatidylglycerol is probably not due to higher-affinity interactions with the TCRs; rather, it may be attributable to improved loading and/or binding to CD1d.

Table III. Reactivity of dNKT hybridomas to *Listeria* phosphatidylglycerol–LC-MS fraction E

Hybridoma	RAW-CD1d APCs	Plate-Bound CD1d
14S.6	+	+
14S.10	+	+
14S.15	−	−
431.A11	−	−
TBA7	+	+
VII68	+	−
VIII24.1.D	+	−
XV19.2	−	−

Reactivity to *Listeria* phosphatidylglycerol LC-MS fraction E was tested in APC-containing (RAW-CD1d cells) and APC-free (plate-bound CD1d) systems.
+, reactive; −, not reactive.

Discussion

There is a growing appreciation that many T cells do not recognize peptides in the context of MHC class I or MHC class II molecules (47). Such non-MHC–restricted T cells, which can recognize lipid Ags (48) or riboflavin metabolites (49), include NKT cells (CD1d restricted), mucosal-associated invariant T cells (MR1 restricted), CD1a/CD1b/CD1c T cells, and TCR γδ T cells. Collectively, these cells can represent between 10 and 50% of circulating T lymphocytes, depending on the human donor (10, 50–53). By using CD1 or MR1 multimers loaded with specific Ags, investigators have started to interrogate these non-MHC–restricted T cell populations in vivo (43, 52, 54).

Primary dNKT cells are poorly understood because of the lack of tools to identify them in vivo (55). dNKT cells restricted against the mammalian lipid sulfatide is the only primary dNKT cell population that has been carefully studied ex vivo with CD1d tetramers (12, 56). However, because of the wide range of TCR Vα- and Vβ-chains used by dNKT cells, it is unlikely that the function(s) of sulfatide-restricted dNKT cells can be generalized to all dNKT cells. Indeed, the dNKT XV19 hybridoma, which recognizes sulfatide and was the basis for testing sulfatide-loaded CD1d tetramers, does not recognize the *Listeria* phosphatidylglycerol Ags used in this study (Table III, data not shown). This finding highlights the need to identify more high-potency dNKT cell Ags for further interrogation of dNKT cells in vivo.

Microbial lipid Ags are ideal targets for dNKT cells. Although mammalian self-lipids may be responsible for dNKT cell selection in the thymus, like self-peptides for MHC-restricted T cells, the most potent Ags recognized in the periphery may be of microbial origin. Because *Listeria* is an intracellular microbial pathogen, it was an attractive model organism for identifying Ags for dNKT cells (29, 57). By performing an unbiased search for *Listeria* lipid Ags, we identified the microbial versions of two known dNKT cell phospholipid Ags, phosphatidylglycerol and DPG, as dNKT cell Ags. By measuring the concentration of *Listeria* phosphatidylglycerol needed to activate 14S.6 and TBA7 hybridoma cells as compared to phosphatidylglycerol-Cg (Fig. 4B), we found that *Listeria* phosphatidylglycerol is a 10–100-fold more potent Ag than the previously published mammalian or the structurally related *Corynebacterium* phosphatidylglycerol.

These results prompted us to consider why *Listeria* phosphatidylglycerol is a more potent Ag than the structurally similar *Corynebacterium*/mammalian phosphatidylglycerol. Because these two lipids share identical headgroups, it was unsurprising to find that the dNKT TBA7 TCR bound to CD1d loaded with either *Listeria* or *Corynebacterium* phosphatidylglycerol with similar affinities. However, we found that *Listeria* phosphatidylglycerol loaded into CD1d (displacing the charged lipid GD3) ∼2-fold more efficiently than did *Corynebacterium* phosphatidylglycerol. Because TCR activation leads to signaling cascades that can exponentially amplify the original signal, we attribute the higher potency of *Listeria* phosphatidylglycerol to its increased CD1d loading efficiency over *Corynebacterium* phosphatidylglycerol. However, we cannot discount the possibility that *Listeria* phos-

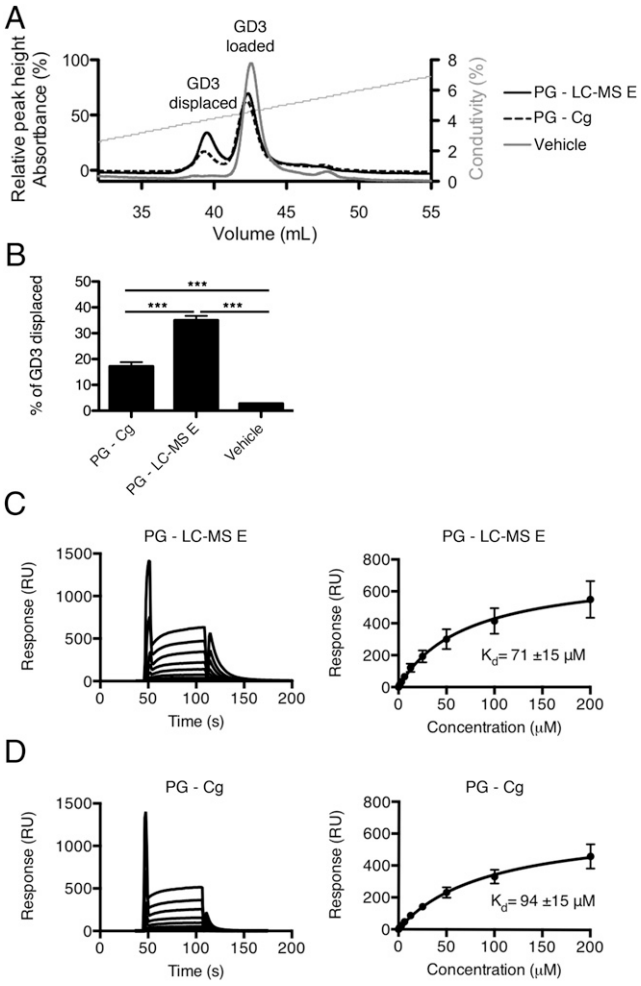

FIGURE 6. *Listeria* phosphatidylglycerol loads into CD1d more efficiently than *Corynebacterium* phosphatidylglycerol. (**A**) Mono-Q anion-exchange–purified GD3-loaded CD1d was incubated overnight with *Listeria* or *Corynebacterium* phosphatidylglycerol at a 30:1 molar ratio of phosphatidylglycerol/GD3-CD1d; 0.05% tyloxapol vehicle control also was used to determine spontaneous GD3 displacement. The displacement of GD3 in each condition was determined by MonoQ anion-exchange chromatography using fast protein liquid chromatography. Conductivity (thin light gray line) denotes the increasing salt concentration added to the column and is used to allow for overlaying different chromatograms. (**B**) The heights of the nondisplaced and displaced peaks from three independent experiments were converted into percentage displacement. SPR was performed as follows: *Listeria* phosphatidylglycerol-LC-MS fraction E loaded CD1d-biotin (**C**) or *Corynebacterium* phosphatidylglycerol loaded CD1d-biotin (**D**) was first purified as shown in (A) and then immobilized to a streptavidin-coated SPR chip. Soluble TBA7 TCR was passed over the chip at various concentrations (200–0.78 μM). TBA7 TCR binding (measured in RU) over time at different concentrations (*left panels*). Equilibrium affinity analysis used to determine K_D (*right panels*). Data in (A) are representative of three independent experiments, with collective data from the three experiments depicted in (B). Data in (C) and (D) show results from duplicate runs from one of two independent experiments. Data in (B) and the *right panels* in (C) and (D) are mean ± SEM. ***$p < 0.001$, one-way ANOVA.

phatidylglycerol is more stably bound within CD1d over time as compared to *Corynebacterium* phosphatidylglycerol.

There are three differences between the fatty acid tails found in *Listeria* that could be modulating its ability to load or stay within CD1d more efficiently than mammalian phosphatidylglycerol. These differences include the presence of anteiso methyl groups, lack of a double bond, and shorter tail lengths. One hypothesis is that the anteiso methyl fatty acid branches (found only in some microbes) act as a hook within the CD1d hydrophobic channels and increase the stability of the lipid–CD1d complex. Alternatively, it is possible that other aspects of *Listeria* phosphatidylglycerol, such as its shorter tails or lack of a double bond, make it easier to load or remain bound within CD1d molecules.

Our previous attempts to generate *Corynebacterium* or mammalian phosphatidylglycerol CD1d tetramers were not successful. However, identification of the more potent *Listeria* phosphatidylglycerol variant prompted us to determine whether CD1d tetramers loaded with *Listeria* phosphatidylglycerol could bind with sufficient avidity to TBA7 cells to stain in flow cytometry. Indeed, *Listeria* phosphatidylglycerol–LC-MS fraction E–loaded CD1d tetramers specifically bound to TBA7 TCR-transduced cells but not to the same cells transduced with other (or no) TCRs (Fig. 5C, 5D, data not shown). By using dextramers that contain ~12 CD1d molecules and multiple fluorophores/molecule, we were able to further increase the signal/noise ratio so that the majority of the *Listeria* phosphatidylglycerol dextramer-stained cells could be separated from the mock- or irrelevant lipid–loaded dextramer-stained cells. This increase in signal may be critical, because it provides a new reagent that is suitable to identify and interrogate dNKT cells in vivo. We are now optimizing this technology to stain primary human and mouse dNKT cells, including taking advantage of the recent insight that unlabeled anti-fluorophore Abs can stabilize TCR–multimer complexes with affinities similar to those found in this study (58).

In summary, we identified a new lipid Ag for dNKT cells with a distinctively microbial signature: short, fully saturated anteiso lipid tails. Notably, this microbial version of phosphatidylglycerol is much more active than the previously known phosphatidylglycerol Ags from mammals or *Corynebacterium*, which have structurally related lipid tails. Importantly, by identifying high-potency microbial dNKT cell Ags for different dNKT cell populations, we can begin to dissect the poorly understood nature of dNKT cells in vivo.

Acknowledgments

We thank the National Institutes of Health Tetramer Core Facility (contract HHSN272201300006C) for providing us with unloaded biotinylated CD1d monomers and the PBS-57 tetramer. We also thank Xavier Michelet, Sook Kyung Chang, Patrick Brennan, Daniel Pellicci, and other members of the Brenner, Godfrey, and Rossjohn laboratories for helpful discussions, support, and advice. Finally, we are grateful to Søren Jakobsen at Immudex for supplying us with dextramer backbones.

Disclosures

The authors have no financial conflicts of interest.

References

1. Cohen, N. R., S. Garg, and M. B. Brenner. 2009. Antigen Presentation by CD1 Lipids, T Cells, and NKT Cells in Microbial Immunity. Adv. Immunol. 102: 1–94.
2. Benlagha, K., A. Weiss, A. Beavis, L. Teyton, and A. Bendelac. 2000. In vivo identification of glycolipid antigen-specific T cells using fluorescent CD1d tetramers. *J. Exp. Med.* 191: 1895–1903.
3. Rossjohn, J., D. G. Pellicci, O. Patel, L. Gapin, and D. I. Godfrey. 2012. Recognition of CD1d-restricted antigens by natural killer T cells. *Nat. Rev. Immunol.* 12: 845–857.
4. Scott-Browne, J. P., J. L. Matsuda, T. Mallevaey, J. White, N. A. Borg, J. McCluskey, J. Rossjohn, J. Kappler, P. Marrack, and L. Gapin. 2007. Germline-encoded recognition of diverse glycolipids by natural killer T cells. *Nat. Immunol.* 8: 1105–1113.
5. Borg, N. A., K. S. Wun, L. Kjer-Nielsen, M. C. Wilce, D. G. Pellicci, R. Koh, G. S. Besra, M. Bharadwaj, D. I. Godfrey, J. McCluskey, and J. Rossjohn. 2007. CD1d-lipid-antigen recognition by the semi-invariant NKT T-cell receptor. *Nature* 448: 44–49.
6. Patel, O., D. G. Pellicci, S. Gras, M. L. Sandoval-Romero, A. P. Uldrich, T. Mallevaey, A. J. Clarke, J. Le Nours, A. Theodossis, S. L. Cardell, et al. 2012. Recognition of CD1d-sulfatide mediated by a type II natural killer T cell antigen receptor. *Nat. Immunol.* 13: 857–863.
7. Girardi, E., I. Maricic, J. Wang, T.-T. Mac, P. Iyer, V. Kumar, and D. M. Zajonc. 2012. Type II natural killer T cells use features of both innate-like and conventional T cells to recognize sulfatide self antigens. *Nat. Immunol.* 13: 851–856.
8. Uldrich, A. P., J. Le Nours, D. G. Pellicci, N. A. Gherardin, K. G. McPherson, R. T. Lim, O. Patel, T. Beddoe, S. Gras, J. Rossjohn, and D. I. Godfrey. 2013. CD1d-lipid antigen recognition by the γδ TCR. *Nat. Immunol.* 14: 1137–1145.
9. Pellicci, D. G., A. P. Uldrich, J. Le Nours, F. Ross, E. Chabrol, S. B. Eckle, R. de Boer, R. T. Lim, K. McPherson, G. Besra, et al. 2014. The molecular bases of δ/αβ T cell-mediated antigen recognition. *J. Exp. Med.* 211: 2599–2615.
10. Rhost, S., S. Sedimbi, N. Kadri, and S. L. Cardell. 2012. Immunomodulatory type II natural killer T lymphocytes in health and disease. *Scand. J. Immunol.* 76: 246–255.
11. Maricic, I., E. Girardi, D. M. Zajonc, and V. Kumar. 2014. Recognition of lysophosphatidylcholine by type II NKT cells and protection from an inflammatory liver disease. *J. Immunol.* 193: 4580–4589.
12. Jahng, A., I. Maricic, C. Aguilera, S. Cardell, R. C. Halder, and V. Kumar. 2004. Prevention of autoimmunity by targeting a distinct, noninvariant CD1d-reactive T cell population reactive to sulfatide. *J. Exp. Med.* 199: 947–957.
13. Tatituri, R. V., G. F. Watts, V. Bhowruth, N. Barton, A. Rothchild, F.-F. Hsu, C. F. Almeida, L. R. Cox, L. Eggeling, S. Cardell, et al. 2013. Recognition of microbial and mammalian phospholipid antigens by NKT cells with diverse TCRs. *Proc. Natl. Acad. Sci. USA* 110: 1827–1832.
14. Rhost, S., L. Löfbom, B.-M. Rynmark, B. Pei, J.-E. Månsson, S. Teneberg, M. Blomqvist, and S. L. Cardell. 2012. Identification of novel glycolipid ligands activating a sulfatide-reactive, CD1d-restricted, type II natural killer T lymphocyte. *Eur. J. Immunol.* 42: 2851–2860.
15. Gumperz, J. E., C. Roy, A. Makowska, D. Lum, M. Sugita, T. Podrebarac, Y. Koezuka, S. A. Porcelli, S. Cardell, M. B. Brenner, and S. M. Behar. 2000. Murine CD1d-restricted T cell recognition of cellular lipids. *Immunity* 12: 211–221.
16. Makowska, A., T. Kawano, M. Taniguchi, and S. Cardell. 2000. Differences in the ligand specificity between CD1d-restricted T cells with limited and diverse T-cell receptor repertoire. *Scand. J. Immunol.* 52: 71–79.
17. Chang, D. H., H. Deng, P. Matthews, J. Krasovsky, G. Ragupathi, R. Spisek, A. Mazumder, D. H. Vesole, S. Jagannath, and M. V. Dhodapkar. 2008. Inflammation-associated lysophospholipids as ligands for CD1d-restricted T cells in human cancer. *Blood* 112: 1308–1316.
18. Zeissig, S., K. Murata, L. Sweet, J. Publicover, Z. Hu, A. Kaser, E. Bosse, J. Iqbal, M. M. Hussain, K. Balschun, et al. 2012. Hepatitis B virus-induced lipid alterations contribute to natural killer T cell-dependent protective immunity. *Nat. Med.* 18: 1060–1068.
19. Nair, S., C. S. Boddupalli, R. Verma, J. Liu, R. Yang, G. M. Pastores, P. K. Mistry, and M. V. Dhodapkar. 2015. Type II NKT-TFH cells against Gaucher lipids regulate B-cell immunity and inflammation. *Blood* 125: 1256–1271.
20. Cui, J., T. Shin, T. Kawano, H. Sato, E. Kondo, I. Toura, Y. Kaneko, H. Koseki, M. Kanno, and M. Taniguchi. 1997. Requirement for Valpha14 NKT cells in IL-12-mediated rejection of tumors. *Science* 278: 1623–1626.
21. Exley, M. A., N. J. Bigley, O. Cheng, A. Shaulov, S. M. A. Tahir, Q. L. Carter, J. Garcia, C. Wang, K. Patten, H. F. Stills, et al. 2003. Innate immune response to encephalomyocarditis virus infection mediated by CD1d. *Immunology* 110: 519–526.
22. Bedel, R., J. L. Matsuda, M. Brigl, J. White, J. Kappler, P. Marrack, and L. Gapin. 2012. Lower TCR repertoire diversity in Traj18-deficient mice. *Nat. Immunol.* 13: 705–706.
23. Neuenhahn, M., K. M. Kerksiek, M. Nauerth, M. H. Suhre, M. Schiemann, F. E. Gebhardt, C. Stemberger, K. Panthel, S. Schröder, T. Chakraborty, et al. 2006. CD8alpha+ dendritic cells are required for efficient entry of *Listeria monocytogenes* into the spleen. *Immunity* 25: 619–630.
24. Rosen, H., S. Gordon, and R. J. North. 1989. Exacerbation of murine listeriosis by a monoclonal antibody specific for the type 3 complement receptor of myelomonocytic cells. Absence of monocytes at infective foci allows *Listeria* to multiply in nonphagocytic cells. *J. Exp. Med.* 170: 27–37.
25. Wollert, T., B. Pasche, M. Rochon, S. Deppenmeier, J. van den Heuvel, A. D. Gruber, D. W. Heinz, A. Lengeling, and W.-D. Schubert. 2007. Extending the host range of *Listeria monocytogenes* by rational protein design. *Cell* 129: 891–902.
26. Hamon, M., H. Bierne, and P. Cossart. 2006. *Listeria monocytogenes*: a multifaceted model. *Nat. Rev. Microbiol.* 4: 423–434.
27. Arrunategui-Correa, V., and H. S. Kim. 2004. The role of CD1d in the immune response against *Listeria* infection. *Cell. Immunol.* 227: 109–120.
28. Ranson, T., S. Bregenholt, A. Lehuen, O. Gaillot, M. C. Leite-de-Moraes, A. Herbelin, P. Berche, and J. P. Di Santo. 2005. Invariant V alpha 14+ NKT cells participate in the early response to enteric *Listeria monocytogenes* infection. *J. Immunol.* 175: 1137–1144.
29. Fischer, W., and K. Leopold. 1999. Polar lipids of four *Listeria* species containing L-lysylcardiolipin, a novel lipid structure, and other unique phospholipids. *Int. J. Syst. Bacteriol.* 49: 653–662.

30. Cohen, N. R., R. V. Tatituri, A. Rivera, G. F. Watts, E. Y. Kim, A. Chiba, B. B. Fuchs, E. Mylonakis, G. S. Besra, S. M. Levitz, et al. 2011. Innate recognition of cell wall β-glucans drives invariant natural killer T cell responses against fungi. *Cell Host Microbe* 10: 437–450.
31. Cardell, S., S. Tangri, S. Chan, M. Kronenberg, C. Benoist, and D. Mathis. 1995. CD1-restricted CD4+ T cells in major histocompatibility complex class II-deficient mice. *J. Exp. Med.* 182: 993–1004.
32. Behar, S. M., T. A. Podrebarac, C. J. Roy, C. R. Wang, and M. B. Brenner. 1999. Diverse TCRs recognize murine CD1. *J. Immunol.* 162: 161–167.
33. Park, S. H., A. Weiss, K. Benlagha, T. Kyin, L. Teyton, and A. Bendelac. 2001. The mouse CD1d-restricted repertoire is dominated by a few autoreactive T cell receptor families. *J. Exp. Med.* 193: 893–904.
34. Lantz, O., and A. Bendelac. 1994. An invariant T cell receptor alpha chain is used by a unique subset of major histocompatibility complex class I-specific CD4+ and CD4-8- T cells in mice and humans. *J. Exp. Med.* 180: 1097–1106.
35. Letourneur, F., and B. Malissen. 1989. Derivation of a T cell hybridoma variant deprived of functional T cell receptor alpha and beta chain transcripts reveals a nonfunctional alpha-mRNA of BW5147 origin. *Eur. J. Immunol.* 19: 2269–2274.
36. Brigl, M., R. V. Tatituri, G. F. Watts, V. Bhowruth, E. A. Leadbetter, N. Barton, N. R. Cohen, F.-F. Hsu, G. S. Besra, and M. B. Brenner. 2011. Innate and cytokine-driven signals, rather than microbial antigens, dominate in natural killer T cell activation during microbial infection. *J. Exp. Med.* 208: 1163–1177.
37. Tatituri, R. V., B. J. Wolf, M. B. Brenner, J. Turk, and F.-F. Hsu. 2015. Characterization of polar lipids of *Listeria monocytogenes* by HCD and low-energy CAD linear ion-trap mass spectrometry with electrospray ionization. *Anal. Bioanal. Chem.* 407: 2519–2528.
38. Pellicci, D. G., O. Patel, L. Kjer-Nielsen, S. S. Pang, L. C. Sullivan, K. Kyparissoudis, A. G. Brooks, H. H. Reid, S. Gras, I. S. Lucet, et al. 2009. Differential recognition of CD1d-α-galactosyl ceramide by the V β 8.2 and V β 7 semi-invariant NKT T cell receptors. *Immunity* 31: 47–59.
39. Garboczi, D. N., U. Utz, P. Ghosh, A. Seth, J. Kim, E. A. VanTienhoven, W. E. Biddison, and D. C. Wiley. 1996. Assembly, specific binding, and crystallization of a human TCR-alphabeta with an antigenic Tax peptide from human T lymphotropic virus type 1 and the class I MHC molecule HLA-A2. *J. Immunol.* 157: 5403–5410.
40. Arrunategui-Correa, V., L. Lenz, and H. S. Kim. 2004. CD1d-independent regulation of NKT cell migration and cytokine production upon *Listeria monocytogenes* infection. *Cell. Immunol.* 232: 38–48.
41. Kaneda, T. 1991. Iso- and anteiso-fatty acids in bacteria: biosynthesis, function, and taxonomic significance. *Microbiol. Rev.* 55: 288–302.
42. Batard, P., D. A. Peterson, E. Devêvre, P. Guillaume, J.-C. Cerottini, D. Rimoldi, D. E. Speiser, L. Winther, and P. Romero. 2006. Dextramers: new generation of fluorescent MHC class I/peptide multimers for visualization of antigen-specific CD8+ T cells. *J. Immunol. Methods* 310: 136–148.
43. Kasmar, A. G., I. Van Rhijn, K. G. Magalhaes, D. C. Young, T.-Y. Cheng, M. T. Turner, A. Schiefner, R. C. Kalathur, I. A. Wilson, M. Bhati, et al. 2013. Cutting Edge: CD1a tetramers and dextramers identify human lipopeptide-specific T cells ex vivo. *J. Immunol.* 191: 4499–4503.
44. Venkataswamy, M. M., and S. A. Porcelli. 2010. Lipid and glycolipid antigens of CD1d-restricted natural killer T cells. *Semin. Immunol.* 22: 68–78.
45. Wun, K. S., G. Cameron, O. Patel, S. S. Pang, D. G. Pellicci, L. C. Sullivan, S. Keshipeddy, M. H. Young, A. P. Uldrich, M. S. Thakur, et al. 2011. A molecular basis for the exquisite CD1d-restricted antigen specificity and functional responses of natural killer T cells. *Immunity* 34: 327–339.
46. McCarthy, C., D. Shepherd, S. Fleire, V. S. Stronge, M. Koch, P. A. Illarionov, G. Bossi, M. Salio, G. Denkberg, F. Reddington, et al. 2007. The length of lipids bound to human CD1d molecules modulates the affinity of NKT cell TCR and the threshold of NKT cell activation. *J. Exp. Med.* 204: 1131–1144.
47. Rossjohn, J., S. Gras, J. J. Miles, S. J. Turner, D. I. Godfrey, and J. McCluskey. 2015. T cell antigen receptor recognition of antigen-presenting molecules. *Annu. Rev. Immunol.* 33: 169–200.
48. Brigl, M., and M. B. Brenner. 2004. CD1: antigen presentation and T cell function. *Annu. Rev. Immunol.* 22: 817–890.
49. Kjer-Nielsen, L., O. Patel, A. J. Corbett, J. Le Nours, B. Meehan, L. Liu, M. Bhati, Z. Chen, L. Kostenko, R. Reantragoon, et al. 2012. MR1 presents microbial vitamin B metabolites to MAIT cells. *Nature* 491: 717–723.
50. Dusseaux, M., E. Martin, N. Serriari, I. Péguillet, V. Premel, D. Louis, M. Milder, L. Le Bourhis, C. Soudais, E. Treiner, and O. Lantz. 2011. Human MAIT cells are xenobiotic-resistant, tissue-targeted, CD161hi IL-17-secreting T cells. *Blood* 117: 1250–1259.
51. de Jong, A., V. Peña-Cruz, T.-Y. Cheng, R. A. Clark, I. Van Rhijn, and D. B. Moody. 2010. CD1a-autoreactive T cells are a normal component of the human αβ T cell repertoire. *Nat. Immunol.* 11: 1102–1109.
52. Reantragoon, R., A. J. Corbett, I. G. Sakala, N. A. Gherardin, J. B. Furness, Z. Chen, S. B. G. Eckle, A. P. Uldrich, R. W. Birkinshaw, O. Patel, et al. 2013. Antigen-loaded MR1 tetramers define T cell receptor heterogeneity in mucosal-associated invariant T cells. *J. Exp. Med.* 210: 2305–2320.
53. Bonneville, M., R. L. O'Brien, and W. K. Born. 2010. Gammadelta T cell effector functions: a blend of innate programming and acquired plasticity. *Nat. Rev. Immunol.* 10: 467–478.
54. Ly, D., A. G. Kasmar, T. Y. Cheng, A. de Jong, S. Huang, S. Roy, A. Bhatt, R. P. van Summeren, J. D. Altman, W. R. Jacobs, Jr., et al. 2013. CD1c tetramers detect ex vivo T cell responses to processed phosphomycoketide antigens. *J. Exp. Med.* 210: 729–741.
55. Salio, M., J. D. Silk, E. Y. Jones, and V. Cerundolo. 2014. Biology of CD1- and MR1-restricted T cells. *Annu. Rev. Immunol.* 32: 323–366.
56. Arrenberg, P., R. Halder, Y. Dai, I. Maricic, and V. Kumar. 2010. Oligoclonality and innate-like features in the TCR repertoire of type II NKT cells reactive to a beta-linked self-glycolipid. *Proc. Natl. Acad. Sci. USA* 107: 10984–10989.
57. Sun, Y., and M. X. O'Riordan. 2010. Branched-chain fatty acids promote *Listeria monocytogenes* intracellular infection and virulence. *Infect. Immun.* 78: 4667–4673.
58. Tungatt, K., V. Bianchi, M. D. Crowther, W. E. Powell, A. J. Schauenburg, A. Trimby, M. Donia, J. J. Miles, C. J. Holland, D. K. Cole, et al. 2015. Antibody stabilization of peptide-MHC multimers reveals functional T cells bearing extremely low-affinity TCRs. *J. Immunol.* 194: 463–474.